Supporting Information to

Interfacial pH Measurements during CO$_2$ Reduction Using a Rotating Ring-Disk Electrode

Xuan Liu[a], Mariana C. O. Monteiro[a,b], and Marc T. M. Koper[a]*

[a]Leiden Institute of Chemistry, Leiden University, 2300 RA Leiden, The Netherlands

[b]Current address: Interface Science Department, Fritz Haber Institute of the Max Planck Society, 14195 Berlin, Germany

Cyclic voltammograms of 4-NTP reduction

As shown in Figure S1a, before measurements, to confirm the cleanliness of the electrodes and measure the ECSA, both ring and disk electrodes were characterized in Ar-saturated 0.1 M H_2SO_4 by cyclic voltammetry between 0 and 1.75 V vs RHE. After that, the gold ring was modified with the 4-NTP molecule, and then the 4-NTP was converted into the pH sensing redox couple 4-NSTP/4-HATP using a voltammetry in 0.1 M H_2SO_4 from 0.68 V vs RHE at 100 mV s^{-1} (Figure S1b). During the negative-going potential sweep, part of the 4-NTP is reduced completely to 4-ATP through a 6-proton-6-electron pathway, [1] while some 4-NTP was reduced partially to the 4-NSTP through a 4-proton-4-electron pathway, and the 4-NSTP is re-oxidized to 4-HATP in the positive-going potential sweep (Figure S1c). [2] As intermediates of the reduction, the content of 4-NSTP/4-HATP drops with decreasing lower vertex potentials (Figure S1d). Therefore, 0.11V vs RHE was used as lower vertex potential to optimize signals from the redox couple.
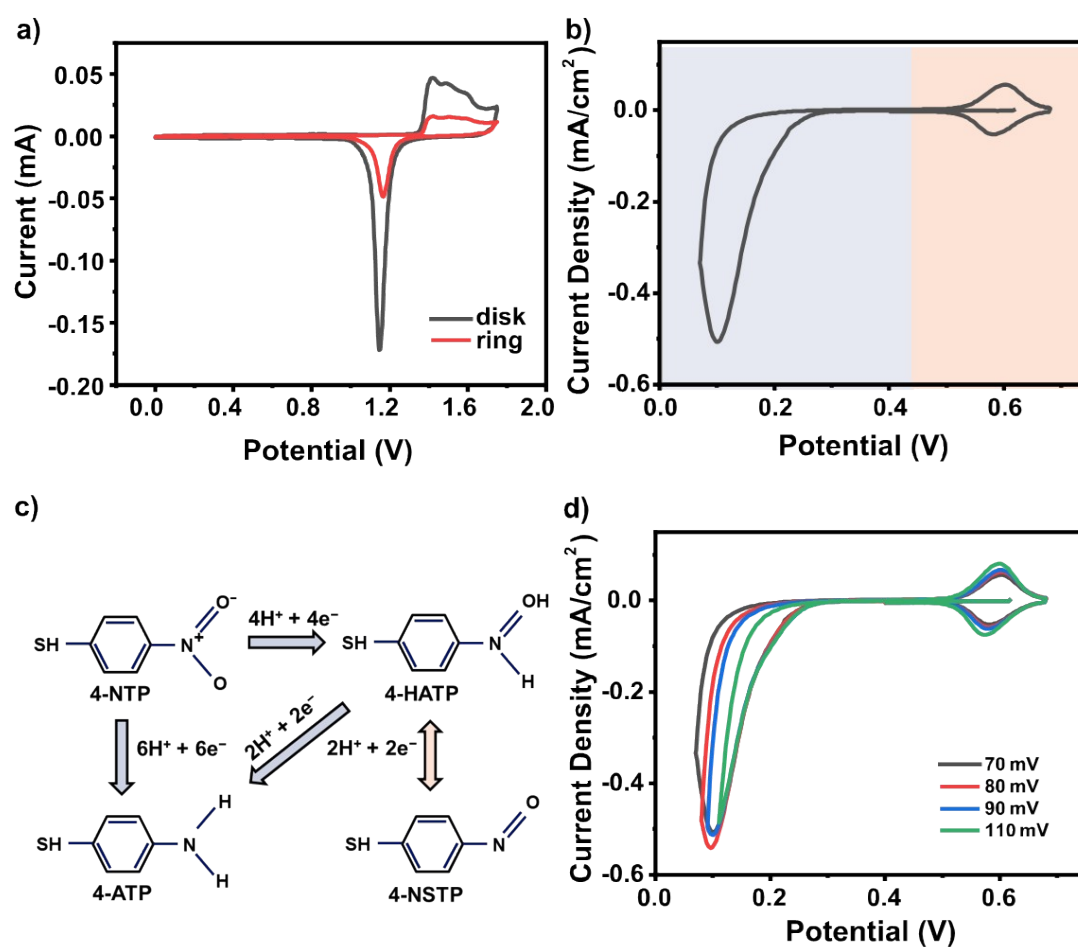
Figure S1. a) Blank voltammograms of the ring (black) and disc (red) electrodes taken in 0.1 M H_2SO_4 at 100 mV s^{-1} . **b)** the Voltammogram of conversion from 4-NTP to the 4-NSTP/4-HATP redox couple in Ar-saturated 0.1M H_2SO_4 at 100mV/s. **c)** scheme of the reduction pathways of 4-NTP; **d)** Reduction of 4-NTP with different vertex potentials during cyclic voltammetry in Ar-saturated 0.1M H_2SO_4 at 100mV/s.

Calibration Curve

The peak potentials of the pH redox couple were measured by cyclic voltammetry in electrolytes with different pH. The alkaline region was measured in 0.1 M $KHCO_3$ with pH adjusted by adding KOH or purging CO_2. The acidic region was measured in CO_2 saturated 0.1 M $NaClO_4$. pH was measured by a pH meter (lab 855, SI Analytics)
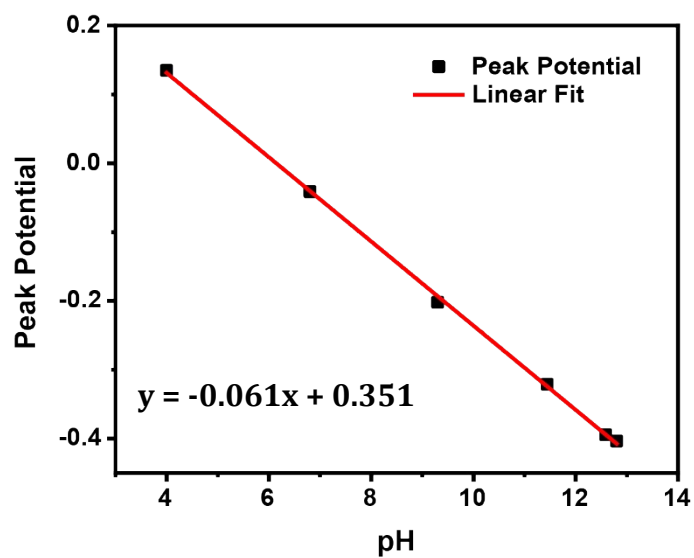
Figure S2. Calibration curve of the 4-NSTP/4-HATP redox couple.

Calculation of the interfacial pH

The interfacial pH at the disk was deduced from the peak potential of the 4-NSTP/4-HATP pH sensing couple. During RRDE measurements, cyclic voltammograms of the 4-HATP/4-NSTP modified Au ring were constantly recorded, the peak potentials of which shifted negatively with the increasing pH (Figure S3a). Firstly, these peak potentials were determined by fitting the anodic scans with a Gaussian function with a linear background. Using the calibration curve (pH_{RING} = (0.351 − E)/ 0.061, see Figure S2b), interfacial pH on the ring electrode was obtained from the peak potential (Figure S3b). Then, the interfacial pH of the disk electrode was calculated according to the well-defined concentration profile of RRDE, developed from the convective diffusion equation by Albery and Calvo. [3] The ratio between the average concentration of products on the ring and the disk is defined as the detection efficiency N_D (Eq. s2), where μ is the normalized concentration of products (Eq. s1), C_∞ is the bulk concentration and subscripts "d" and "r" stand for the ring and disk electrode, respectively. N_D depends only on the geometry of the electrode (Eqs. s3-4), where r_1, r_2 and r_3 are the radii of the disk, the inner ring and the outer ring, respectively. [4] In our case, the designated product here is OH^-. As the current on the ring is far smaller than on the disk, it is assumed that the electric field from the ring barely influences the concentration profile of OH^-. Under strong polarization in highly conductive electrolytes, the current distribution within the disk is assumed to be uniform. [5] Consequently, the N_D of the RRDE tip employed here (r_1 = 5.0 mm, r_2 = 6.5 mm, r_3 = 7.5 mm) is calculated to be 0.23 according to Eq. s4. However, in CO_2-saturated bicarbonates, OH^- generated on the disk is partially consumed by either CO_2 or HCO_3^- on its way to the ring. To avoid an underestimation of the interfacial pH on the disk, these homogeneous buffering reactions (Eqs 2 and 4) are taken into account. [6] With effective buffering from CO_2/HCO_3^- and HCO_3^-/CO_3^{2-}, autoprotolysis of water is ignored here. Therefore, the normalized concentration μ here was defined as Eq. s5 and the equation for N_D was also modified (Eq. s6). As CO_2 is continuously purged into the electrolyte during the measurements, the total carbon concentration (TC, see Eq. s7), which is the sum of the concentration of the intrinsic bicarbonate electrolyte and the saturated CO_2 concentration from extrinsic bubbling, stays constant (the TCs for 0.1, 0.25, 0.4 and 0.5 M bicarbonate under continuous CO_2 bubbling are 0.135, 0.271, 0.429, 0.526 M respectively). [7] Concentrations of the different carbonaceous species were estimated as a function of pH (Eqs. s8-s10) by combining equilibrium constants from Eq. 2 and 4 and Eq. s7 ($K_2 = \dfrac{[H^+][HCO_3^-]}{[CO_2]}$, pK$_2$ = 6.35,

$K_4 = \dfrac{[H^+][CO_3^{2-}]}{[HCO_3^-]}$, pK$_2$ = 10.33). [7] As a result, the interfacial pH of the disk electrode was derived from Eqs. S6-s10. The theoretical correlation between the pH on the ring and disk is plotted in Figure S3c. The appearance of two turning points is related to the two buffers in the electrolyte.

$$\mu = (C - C_\infty)/C_\infty \tag{s1}$$

$$N_D = \frac{\mu_r}{\mu_{D,0}} = (C_r - C_\infty)/(C_d - C_\infty) \tag{s2}$$

$$F(\theta) = \frac{3^{\frac{1}{2}}}{4\pi}\ln\left(\frac{\left(1 + \theta^{\frac{1}{3}}\right)^3}{1 + \theta}\right) + \frac{3}{2\pi}\tan^{-1}\left(\frac{2\theta^{\frac{1}{3}} - 1}{3^{\frac{1}{2}}}\right) + \frac{1}{4} \tag{s3}$$

$$N_D = 1 - \frac{1}{6}F\left[\left(\frac{r_2}{r_1}\right)^3 - 1\right] - \frac{2}{3}F\left[\left(\frac{r_2 + r_3}{2r_1}\right)^3 - 1\right] - \frac{1}{6}F\left[\left(\frac{r_3}{r_1}\right)^3 - 1\right] \tag{s4}$$

$$\mu_{OH^-} = \left(C_{OH^-} + C_{HCO_3^-} + 2C_{CO_3^{2-}} - C_{\infty,OH^-} - C_{\infty,HCO_3^-} - 2C_{\infty,CO_3^{2-}} \right) \Big/ \left(C_{\infty,OH^-} + C_{\infty,HCO_3^-} + 2C_{\infty,CO_3^{2-}} \right)$$

(s5)

$$N_D = \frac{\mu_{r,OH^-}}{\mu_{d,OH^-}} = \frac{C_{r,OH^-} + C_{r,HCO_3^-} + 2C_{r,CO_3^{2-}} - C_{\infty,OH^-} - C_{\infty,HCO_3^-} - 2C_{\infty,CO_3^{2-}}}{C_{d,OH^-} + C_{d,HCO_3^-} + 2C_{d,CO_3^{2-}} - C_{\infty,OH^-} - C_{\infty,HCO_3^-} - 2C_{\infty,CO_3^{2-}}}$$

(s6)

$$TC = [CO_2] + [HCO_3^-] + [CO_3^{2-}]$$

(s7)

$$[CO_2] = \frac{TC[H^+]^2}{[H^+]^2 + K_2[H^+] + K_2K_4}$$

(s8)

$$[HCO_3^-] = \frac{TC[H^+]^2}{[H^+]^2 + K_2[H^+] + K_2K_4}$$

(s9)

$$[CO_3^{2-}] = \frac{TC[H^+]^2}{[H^+]^2 + K_2[H^+] + K_2K_4}$$

(s10)
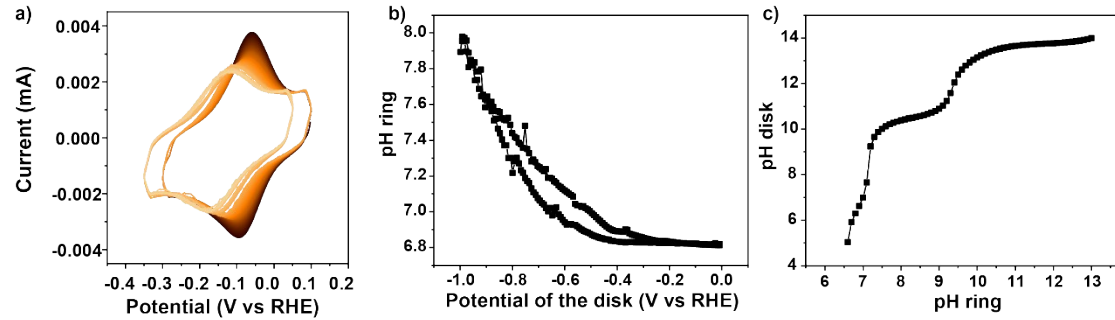
Figure S3. a) Cyclic voltammograms of 4-HATP/4-NSTP modified Au ring electrode during CO_2RR on Au disk electrode in CO_2 saturated 0.1 M $NaHCO_3$ at 2 mV s^{-1} and a rotation rate of 2500 rpm. As the disk was cycling from 0 to − 1.0 V vs RHE, the CVs on the ring evolved from dark red to light and the peak potentials shifted negatively. **b)** Variation of interfacial pH at the ring obtained from peak potentials from a) via calibration curve. **c)** The correspondence between pH$_{ring}$ and pH$_{disk}$ in in CO_2 saturated bicarbonates.

Comparison of our RRDE pH sensor and IrOx

The accuracy and sensitivity of the RRDE pH sensor is highly dependent on the pH-sensitive molecule (or material) present on the ring. Compared with, for example, the recently published IrOx probe from Tackett and co-workers,[8] our pH sensor has higher sensitivity, stability and reproducibility, and wider working range. A direct comparison regarding different properties is given in Table S1 below:

Table S1. Comparison of the pH sensor used by Tackett et al. and in this work:

	This work	**Tackett et al. [8]**
pH-sensitive molecule	4-HATP/4-NSTP redox couple	IrO_x
Signal monitored	Current (voltammetric)	Open circuit potential (Potentiometric)
Type of material	Self-assembled monolayer	μm-thick oxide film
Time resolution	4s per data point	120s per data point
Working range	pH 1-13	pH 2-12
Stability	High (no need of reactivation or recalibration)	• Dependent on the quality of the IrO_x film[9, 10] • Possible dissolution in acidic media[11]
Reproducibility	High[2]	• Dependent on the quality of the IrO_x film • pH probe needs calibration every day
Sensitivity	0.1 pH unit[2]	n.a.

Scan rate dependence experiments in bicarbonate electrolyte

To confirm the equilibrium assumption mentioned above, variations of interfacial pH were recorded with higher scan rates on the disk in CO_2 saturated bicarbonates. As shown in Figure S4a-S4b, the current density increases with scan rate. As a result, accumulation of OH^- near the interface of the electrode increases with scan rate, leading to a higher interfacial pH. The interference from current density makes it difficult to distinguish the scan rate effect.
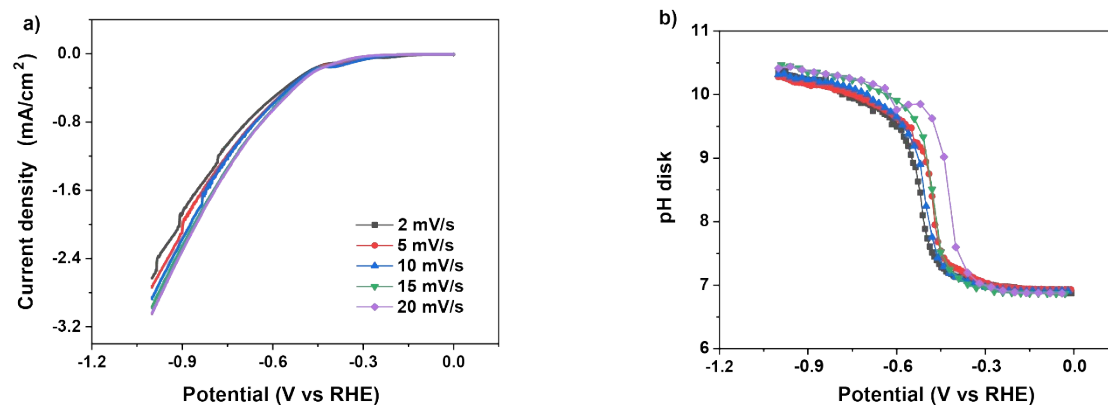
Figure S4. a) Cyclic voltammograms in CO_2 saturated 0.1 M $NaHCO_3$ at different scan rates. The rotation rate of RRDE is 2500 rpm. **b)** Variation of the interfacial pH as a function of potential during cyclic voltammetry in figure 4a.

Variation of concentrations of the carbonaceous species

Variation of concentrations of the carbonaceous species is calculated from the interfacial pH monitored under different conditions. According to the results mentioned above, the current density range can be divided into two parts. In the first range (log j < −1.0 mA cm^{-2}), the interfacial pH is buffered by CO_2/HCO_3^- couple, while the in the second range, the interfacial pH is buffered by HCO_3^-/CO_3^{2-} couple. The results show that increasing mass transport, buffer capacity, and the size and the concentration of cation can resist the variation of interfacial pH: exhaustion of CO_2 and accumulation of HCO_3^- in the CO_2/HCO_3^- buffer range is postponed, and consumption of HCO_3^- and generation of CO_3^{2-} in the HCO_3^-/CO_3^{2-} buffer range is slowed down as well.
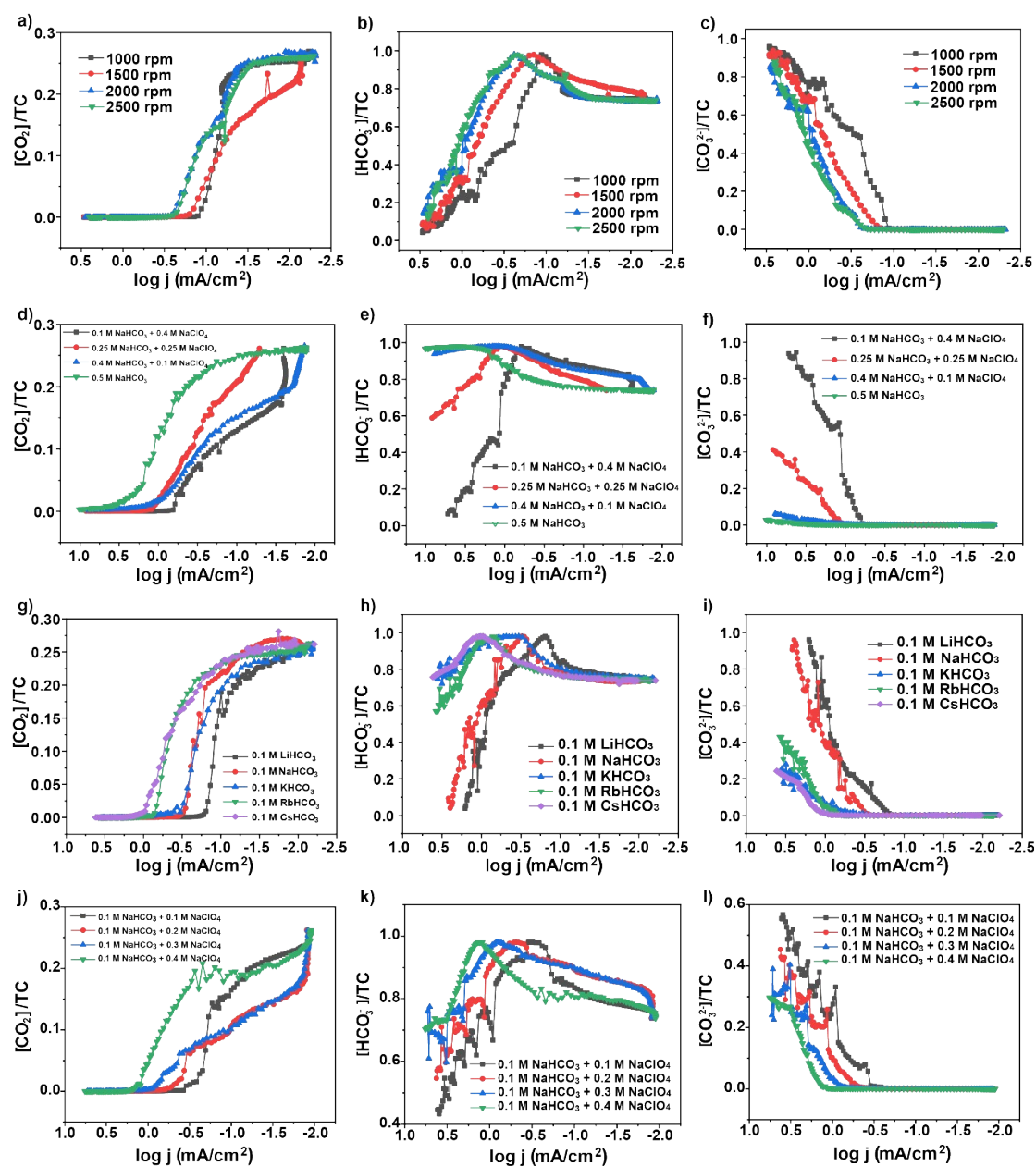
Figure S5. Variation of the interfacial pH as a function of the logarithm of the current density during cyclic voltammetry in **(a-c)** CO_2 saturated 0.1 M $NaHCO_3$ with different rotation rates, **(d-f)** CO_2 saturated bicarbonate with different buffer capacities, **(g-i)** CO_2 saturated bicarbonate with different cations, and **(j-m)** CO_2 saturated bicarbonate with different Na^+ concentrations. The rotation rate is at 2500 rpm except specially mentioned.

Calculation of theoretical limiting current density and thickness of diffusion layer

The limiting current density for CO_2RR (J_L) and thickness of diffusion layer (δ) is calculated according to the Levich equation:

$$J_L = -0.62nFD^{2/3}\omega^{1/2}v^{-1/6}C^*$$

$$\delta = 1.61D^{1/3}\omega^{-1/2}v^{1/6}$$

where n is the number of electrons transferred, F is the Faraday constant (C mol^{-1}), D is the diffusion coefficient (cm^2 s^{-1}), ω is the angular rotation rate (rad s^{-1}), v is the kinematic viscosity (cm^2 s^{-1}) and C is the bulk concentration of the reactant (mol cm^{-3}). For CO_2RR, n is equal to 2. The diffusion coefficient D is $1.95*10^{-5}$ cm^2 s^{-1}. The kinematic viscosity of water is 0.0089 cm^2 s^{-1}. The angular rotation rate of 2500 RPM corresponds to 261.8 rad s^{-1}. The bulk concentration of CO_2 is 35 mM. The calculated limiting current density is 101.41 mA cm^{-2}. The thickness of diffusion layer is 12.24 μm.

References

1. L.-B. Zhao, J.-L. Chen, M. Zhang, D.-Y. Wu and Z.-Q. Tian, *The Journal of Physical Chemistry C*, 2015, **119**, 4949-4958.

2. M. C. O. Monteiro, L. Jacobse, T. Touzalin and M. T. M. Koper, *Anal Chem*, 2020, **92**, 2237-2243.

3. W. Albery, *Transactions of the Faraday Society*, 1966, **62**, 1915-1919.

4. W. J. Albery and E. J. Calvo, *Journal of the Chemical Society, Faraday Transactions 1: Physical Chemistry in Condensed Phases*, 1983, **79**, 2583-2596.

5. W. J. Albery and M. L. Hitchman, *Ring-disc Electrodes [by] W.J. Albery and M.L. Hitchman*, Clarendon Press, 1971.

6. R. E. Zeebe and D. Wolf-Gladrow, *CO2 in seawater: equilibrium, kinetics, isotopes*, Gulf Professional Publishing, 2001.

7. H. Zhong, K. Fujii, Y. Nakano and F. Jin, *The Journal of Physical Chemistry C*, 2014, **119**, 55-61.

8. B. M. Tackett, D. Raciti, N. W. Brady, N. L. Ritzert and T. P. Moffat, *The Journal of Physical Chemistry C*, 2022, **126**, 7456-7467.

9. P. Steegstra and E. Ahlberg, *Journal of Electroanalytical Chemistry*, 2012, **685**, 1-7.

10. P. Steegstra and E. Ahlberg, *Electrochimica Acta*, 2012, **76**, 26-33.

11. P. Jovanovič, N. Hodnik, F. Ruiz-Zepeda, I. Arčon, B. Jozinović, M. Zorko, M. Bele, M. Šala, V. S. Šelih and S. Hočevar, *Journal of the American Chemical Society*, 2017, **139**, 12837-12846.